Journal of Chromatography A 1655 (2021) 462502

Contents lists available at ScienceDirect

Journal of Chromatography A

journal homepage: www.elsevier.com/locate/chroma

# Vortex flow reactor assessment for the purification of monoclonal antibodies from unclarified broths

Redondo Miranda Rosa M, Ibáñez González María J*, Mazzuca Sobczuk Tania, Molina Grima Emilio

*Department of Chemical Engineering, Agrifood Campus of International Excellence (CeiA3), University of Almería, Spain*

ARTICLE INFO

*Article history:*
Received 7 May 2021
Revised 19 August 2021
Accepted 25 August 2021
Available online 28 August 2021

*Keywords:*
Vortex flow reactor
Expanded bed
Péclet number
Antibody
Adsorption
Purification

ABSTRACT

The vortex flow reactor (VFR) can be used in many chemical engineering applications. This paper assesses its novel use in the purification of monoclonal antibodies from cell broth. To this end, the IgG2a antibody was purified from the unclarified fermentation broth of transgenic mouse 55/6 hybridoma cells. Visual experiments showed that the VFR worked in the laminar vortices flow regime and the vortices displaced slightly faster than the axial flow. The VFR has the advantage of creating two sorts of flows: axial flow to produce the expanded bed and an extra vortex flow to avoid channeling and stabilize the expanded bed, the hydrodynamic behavior of which is plug flow with an experimental Pèclet number higher than 20. The pH was adjusted in the untreated fermentation broth, which was directly introduced into the reactor thus reducing the number of stages. The IgG2a purification was carried out in a single device via two steps: antibody adsorption in the expanded bed and antibody elution in the settled bed using Streamline rProtein A. A thirty-fold increase in the high-purity antibody concentration was achieved at the top of the pH5 elution peak with a total recovery of 93.1% (w/w) between elution peaks pH 5 and 3.



## 1. Introduction

The VFR is a promising technology in the chemical engineering and biotechnology field. Its hydrodynamic behavior, such as plug flow or well mixing, along with enhanced mass transfer, makes it suitable for a wide variety of applications including heat exchange [1], polymerization [2,3], particle classification [4], photocatalysis [5,6], reverse osmosis [7], enzymatic reactions [8,9], cell cultivation [10,11] and protein purification [12,13].

The VFR is made up of a stationary outer cylinder and a rotating inner cylinder. The low-speed rotational movement of the inner cylinder creates a Couette flow. When the rate surpasses a critical rotation speed, the bifurcation of the flow creates a series of counter-rotating toroidal vortices identified as Taylor vortices, which occupy the inner cylinder in the form of stacked “donuts” [14]. Each vortex has a characteristic size along the z-axis of approximately the gap width between the cylinders. Increasing the rotation rate, different flow patterns appear - from laminar, wavy, and turbulent vortex flow to turbulent flow with no vortices. This also occurs when changing the hydrodynamic behavior from plug flow to well mixing [15,16].

The use of VFRs for protein adsorption began with Moore and Cooney [17] and Ma and Cooney [12] Both had to deal with flow blockages in the reactor outlet due to the presence of the resin. Ma worked at a high rotation rate causing fluidized adsorbent particles to exit the vortices, hence the need to introduce a mesh and increase the outlet area to decrease the axial velocity and keep the particles inside the reactor. They found that the main reason for this was that the particles were suspended by the vortices instead of by the axial flow.

The nylon mesh that produces the resin blockage was removed from the outlet when changing the vortex flow reactor operating conditions [18]. The adsorbent resin is suspended in the axial flow while regulated by the vortex flow. The VFR behavior is similar to that of a fluidized bed but, in this case, the inner cylinder’s rotation speed can be varied independently of the axial velocity, introducing an additional degree of freedom to the system. This configuration thus provides a sound basis for using the vortex flow reactor as an expanded bed chromatography method that is suitable for biomolecule purification [13]. In that research study, the intracellular biomolecule B-phycoerythrin was purified from a concentrated extract consisting of disrupted *Porphyridium cruentum* cells.

The main objective of this work is to assess the potential use of the VFR in purifying monoclonal antibodies, directly from the cell broth, thus avoiding pretreatments.

* Corresponding author.
*E-mail address:* mjibanez@ual.es (I.G. María J).

https://doi.org/10.1016/j.chroma.2021.462502
0021-9673/

The demand for monoclonal antibodies is steadily increasing due to their great potential in therapeutic and diagnostic applications. The global market for therapeutic monoclonal antibodies was valued at $ 115.2 billion in 2018; it is projected to reach $ 300 billion in 2025 [19]. The monoclonal antibody trade accounts for more than 50% of the total biotech market.

Therefore, monoclonals are a very good example of bulk products that have to be purified efficiently to make their production economically competitive. For this reason, it is important to develop less expensive antibody purification processes with shorter execution times [20].

Using chromatography with Protein A as the adsorbent has traditionally been the most suitable alternative for antibody purification. Currently, research is being carried out to optimize this method, such as that by D'Souza et al. [21], who studied the most appropriate mobile phase for reducing biomass fouling in expanded bed adsorption. Given Protein A's high cost and limited shelf life, other authors, such as Zhang et al. [22], focused on reducing the cost of the resin in the overall purification set up by maximizing its functional lifetime. A multitude of antibody purification systems have been developed, many of which attempt to automate the antibody purification process, decrease the processing time and work with up to five samples in parallel [23–26]. Some of the new methods developed for monoclonal antibody purification are based on precipitation with anionic polyelectrolytes [27], aqueous two-phase systems [28–30] or phenylboronic acid chromatography [31]. Nonetheless, all these works have one common characteristic, the need to include a prior sample preparation step. The samples must be clarified, either by filtration or by centrifugation, before being introduced into the purification system.

The novelty of this research is to apply VFR to the purification of antibodies (as extracellular biomolecules) using Protein A. This equipment provides several benefits when used with classical chromatography: on the one hand, the purification is carried out in two stages (adsorption and elution) and on the other, the samples do not require clarification as they can be introduced directly into the reactor. Therefore, not only is the processing time reduced, but also the cost and complexity of the process. The proposed system seeks to maintain the benefits of Protein A chromatography and improve its shortcomings by using a single device.

To achieve the main objective of this work, an expanded bed vortex flow reactor (EB-VFR) was designed, built, and tested for the adsorption and purification of monoclonal antibodies from an unclarified culture broth. The EB-VFR was applied to the recovery of IgG2a from untreated transgenic mouse 55/6 hybridoma fermentation broth. In this case, it was necessary to design a smaller VFR than those used in previous experiments [13]; to do this, the annular gap was kept constant at 0.45 cm by reducing the diameters of the inner and outer cylinders.

## 2. Experimental

### 2.1. Cell culture

Mouse hybridoma cells designated 55-6 (ATCC CRL-2156), which produce immunoglobulin G subclass 2[a] (IgG2a), were cultivated in PFHM II culture medium (Gibco®) without fetal bovine serum (FBS), supplemented with 100U/mL of penicillin-streptomycin (Gibco®) and 0.125 g/mL of amphotericin B (Gibco®). To isolate the IgG2a in the VFR, batch cultures were performed in a 0.6 L stirred-tank reactor (STR) containing 0.4 L of cell culture medium (Biostat Q, B. BRAUN, Germany). The temperature was controlled at 37°C. The dissolved oxygen concentration was maintained at 50% air saturation by adjusting the air/$O_2$/$N_2$ ratio of the inlet gas. Surface aeration was set to a constant 0.1 L/min to maintain a cell concentration up to $5 \times 10^6$ cells/mL, reaching maximum growth rates between 0.018 and 0.034 $h^{-1}$. The antibody concentration in the culture broth at the end of the fermentation process was maintained at around 32.50 µg IgG2a/mL in batch mode.

**Table 1**
Geometric dimensions of the EB-VFR.

| | |
|---|---|
| $r_o$ (outer cylinder radius), cm | 0.95 |
| $r_i$ (inner cylinder radius), cm | 0.50 |
| $\eta$ (radius ratio, $r_i/r_o$) | 0.526 |
| d (annular gap width, $r_o$-$r_i$), cm | 0.45 |
| $d/r_i$ | 0.90 |
| L (height of the outer cylinder) cm | 95 |
| S (gap area), $cm^2$ | 2.05 |
| H (expanded bed height) | 47-56 |
| Γ (aspect ratio, H/d) | 104-124 |

### 2.2. The EB-VFR design

Fig. 1 shows the EB-VFR used in this work. The main body of the reactor is formed by an outer cylinder of transparent acrylic material (1) which remains static, and an inner steel cylinder (2), both of which are conFig.d concentrically. The inner cylinder rotates at a variable speed depending on the set points assigned to the motor (3) (Heidolph RZR 2102 control Z); its rotation range varies from 0 to 75 rpm. Both cylinders are attached at the base by a bearing that allows the inner cylinder to rotate. The output ports (4) are located along the length of the outer cylinder wall, with a distance between each of 2 cm. In addition, 2 mm above the reactor base on the right side is the liquid feed inlet used during the adsorption process (5), and on the left side, the elution fluid outlet (7), over which a nylon mesh is placed to prevent the escape of the adsorbent material. At the bottom of the reactor, there is an outlet port for removing the adsorption resin (6). Two peristaltic pumps (Minipuls3, Gilson, Middleton, USA) are used to pump the liquid flow. The VFR dimensions are shown in Table 1.

### 2.3. The adsorbent

The adsorbent used was Streamline rProtein A (GE Healthcare, Uppsala, Sweden) which is an affinity adsorbent consisting of a composite material of cross-linked agarose and steel beads with a particle size distribution of 80-165 $\mu$m (123 $\mu$m average particle size). The mean particle density was 1300 kg/$m^3$.

### 2.4. Qualitative determination of monoclonal antibodies

A Mouse Immunoglobulin Isotyping ELISA Kit (Thermo Scientific, Rockford, USA) containing mouse $IgG_1$, $IgG_{2a}$, $IgG_{2b}$, $IgG_3$, IgA, IgM and kappa and lambda light chains was used for class and subclass determination of the monoclonal antibodies in the cell culture. This kit uses ELISA plates with wells pre-coated with specific anti-mouse capture antibodies, which allows one to discern $IgG_1$, $IgG_{2a}$, $IgG_{2b}$, $IgG_3$, IgA, IgM, and between kappa or lambda light chains. The steps were followed as per the manufacturer's instructions.

### 2.5. Determination of antibody concentration

The IgG2a concentration in the cell culture, and the adsorption and wash fractions during the purification process, were measured with the sandwich-type ELISA quantitation set (Bethyl Laboratories, Montgomery, USA) using goat anti-mouse IgG-coated plates and goat anti-mouse IgG peroxidase conjugate as the second antibody. The steps followed and the reagents used were those provided in

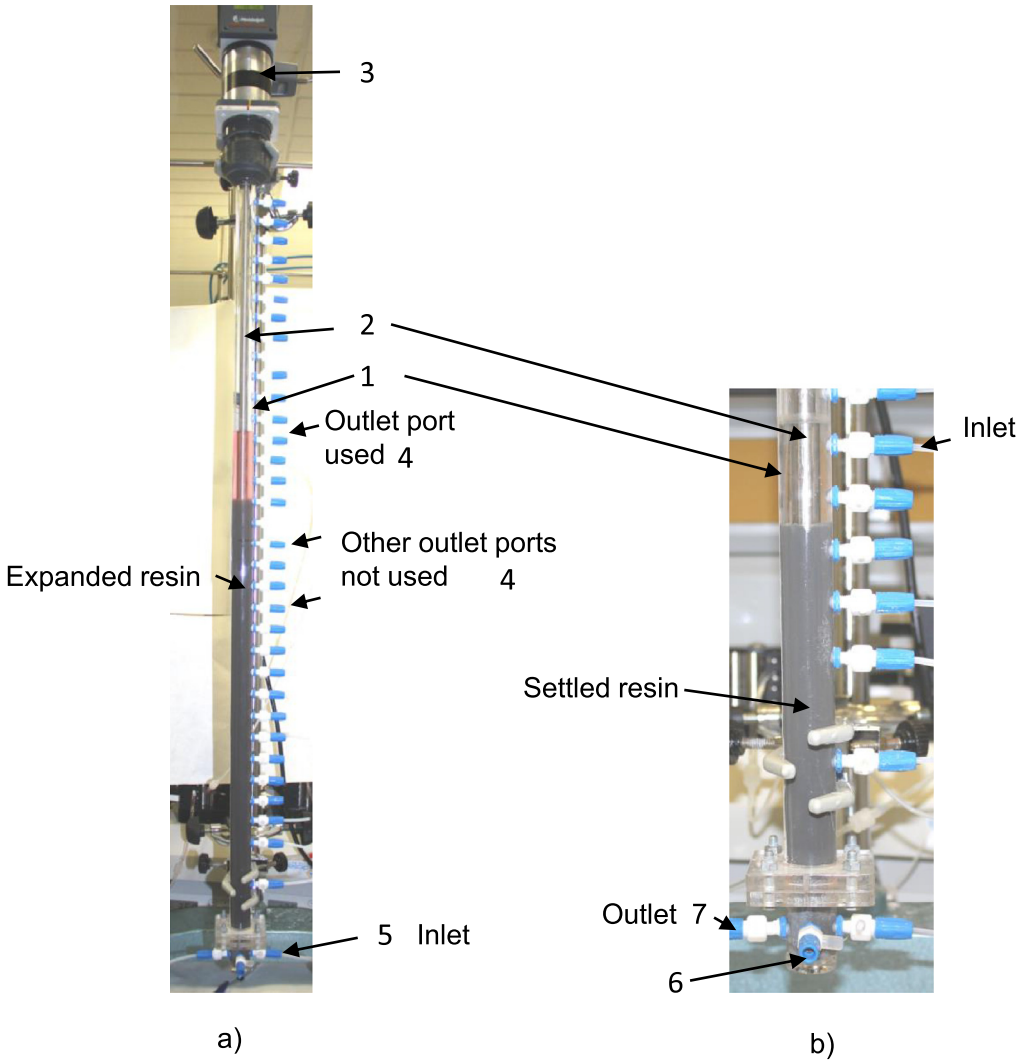


**Fig. 1.** Representation and description of the vortex flow reactor in both phases (a) adsorption with expanded resin, EB-VFR, and (b) elution with settled resin, VFR. (1) clear acrylic outer cylinder, (2) stainless steel inner cylinder, (3) variable speed motor, (4) outlet ports, (5) liquid feed inlet in the adsorption phase, (6) outlet port for removing the adsorbent and (7) outlet port in the elution phase.

the manufacturer's manual. The IgG2a concentration in the elution fractions was calculated by UV adsorption at 280 nm (Jasco V-630, Tokyo, Japan) using a standard curve with standard IgG2a (Bethyl Laboratories, Montgomery, USA). The yield was determined as the loaded antibody percentage that eluted in the purified fractions.

### 2.6. Visualization experiments

Two kinds of visual experiments were performed using pearl mica powder with metal oxides (ferric oxide and titanium dioxide). The particle size distribution was between 10 and 60 $\mu$m and the particle mean density was 2600 kg/m$^3$.

Firstly, the silver pearl mica powder in aqueous suspension (1%) was used to visualize the vortex flow reactor's flow regime at a flow rate of 300 cm/h (10.2 mL/min) and at different rotation rates between 20 and 75 rpm. The suspended particles were mixed before being introduced continuously into the VFR's bottom inlet until stationary conditions were reached at each rotation rate. The suspended particles exited via the outlet port located around 47 cm from the VFR base.

Secondly, a water flow was introduced continuously via the VFR's bottom inlet, which exited via the same outlet port located 47 cm from the bottom of the VFR. After reaching VFR stationary conditions at 300 cm/h, and at different rotation rates between 35 and 75 rpm, 1 mL of red pearl mica in aqueous suspension (1%) was injected by syringe into the port located at a height of 29 cm. Using a ruler situated in the VFR outer cylinder and a timer, it was possible to measure the vortices-pair velocity visualized by the red mica powder. Each assay was performed three times.

### 2.7. Residence time distribution (RTD)

To determine the RTD, the tracer was introduced in steps via the EB-VFR's bottom inlet. The detection of the tracer signal at the reactor outlet determined the RTD of the EB-VFR under the set conditions. The detection was performed by UV absorption set at 280 nm using a spectrophotometer with a flow cell (V630, Jasco, Maryland, USA). The settled bed adsorbent height (Streamline rProtein A) in the annular space was 20 cm (50 mL) and the axial flow rate was 300 cm/h (10.2 mL/min). The expanded bed height was 47 cm.

The residence time distribution (RTD) assays [32] are used to determine the variance by the equation, $\sigma^2 = (\sum_{i=1}^{n} t_i^2 \cdot \Delta C_i/C_{max}) - T^2$, where $\Delta C_i = C_i - C_{i-1}$. $C_i$, $C_{i-1}$ and $C_{max}$ are the tracer concentrations in the VFR outlet at the times $t_i$, $t_{i-1}$ and $t_n$, respec-

tively. The residence time distribution (T, min) is defined as $T = \sum_{i=1}^{n} t_i \cdot \Delta C_i / C_{max}$.

The Péclet number is the ratio of convective to diffusive mass transport, defined as $Pe = U \cdot H / \varepsilon \cdot D_{ax}$, where U is the superficial velocity (m/s), H is the height of the expanded bed (m), $\varepsilon$ is the bed voidage and $D_{ax}$ is the coefficient of axial mixing ($m^2/s$). The Péclet number (Pe) and the axial dispersion ($D_{ax}$, $m^2/s$) were calculated from the RTD assays [33], as explained in the bibliography [13].

RTD analyses were carried out in triplicate at EB-VFR rotation rates of 20, 35, 50 and 75 rpm for rProtein A. Also, an RTD analysis was carried out at 40 rpm and 300 cm/h with no adsorbent, so that the VFR was filled up to a height of 47 cm with water only. The error was calculated as the standard deviation of the triplicate assays.

### 2.8. Frontal chromatography in the expanded bed column

A 0.5 cm column was packed with 1 mL of Streamline rProtein A adsorbent and was further equilibrated with 200 mM of potassium phosphate buffer at pH 7.5. The hybridoma fermentation broth was clarified by centrifugation (10000 g) and microfiltration (0.45 $\mu$m). A 250 mL volume of particle-free solution was adjusted to the pH of the 200 mM sodium phosphate equilibration buffer (pH 7.5) and applied to the column in the expanded bed at an axial flow rate of 300 cm/h. After sample application, the expanded bed was washed with equilibration buffer until no proteins were detected in the column outlet. The bound antibody was eluted in the same column at an axial flow rate of 150 cm/h with 100 mM sodium citrate buffer at different continuous pH values, starting at pH 6 and finishing at pH 3. Finally, adsorbent generation was performed using 2 column volumes of 2 M urea and 2 column volumes of 1 M acetic acid.

### 2.9. Viscosity measurement of the cell culture

A rotational viscometer (Brookfield DV-II + Pro Viscometer, LVF mode, spindle ULA-DIN-85, Middleboro, MA, USA) was used to analyze the rheological parameter of the cell culture.

The experimental values of the shear rate and shear stress data were fitted into the mathematical model, the Power Law, to give the flow behavioral index as $\tau = K \cdot \gamma^n$, where $\tau$ is the shear stress (Pa), K is the consistency index (Pa·s), $\gamma$ is the shear rate ($s^{-1}$) and $n$ is the flow behavior index (dimensionless). When the value of n is equal to 1, the fluid is Newtonian, whereas it is non-Newtonian when n is different from 1. A rotation interval between 50-90 rpm was used with increments of 10 rpm. All samples were analyzed in duplicate at room temperature.

### 2.10. Purification process in the vortex flow reactor

Fig. 3 shows the flowchart of the IgG2a purification, which involved the following steps: mixing the culture with sodium phosphate, adsorption in the EB-VFR, and IgG2a elution in the packed-bed VFR.

The annular space of the vortex flow reactor was filled with 20 cm (50 mL) of Streamline rProtein A adsorbent, which was equilibrated in the upward flow with 200 mM of sodium phosphate, at pH 7.5, and at 300 cm/h (10.2 mL/min). During the equilibration stage, the rotation rate was set at 50 rpm. The equilibration was performed until the expanded bed appeared to be optically stable at an expanded bed height of 47 cm. Later, the pH of the culture (5000 mL, kept frozen at -19°C until use) was adjusted to 7.5 using sodium phosphate and then introduced into the reactor with the same linear flow rate as the equilibration buffer. The expanded bed height increased to 54 cm (Fig. 1a and Fig. 3, step 3). The effluent was gathered in fractions by means of a RediFrac fraction collector (GE Healthcare, Uppsala, Sweden) so that it could be collected in small fractions of a determined volume. The rotation rate of the inner cylinder was 50 rpm.

During the feed application, only the IgG2a antibody was adsorbed into the Streamline rProtein A due to its specificity. Other proteins from the culture medium and the hybridoma cells were eluted. The adsorption process lasted 8 hours. After the feed application, the expanded bed located in the annular space was washed with equilibration buffer until no contaminants could be detected in the outlet flow. Next, the bed was settled in the annular space, and the elution was carried out in packed-bed mode at an axial velocity of 100 cm/h (Fig. 1b and Fig. 3, step 4). The bound IgG2a was eluted with 100 mM sodium citrate buffer at pH 5. Lastly, the remaining adsorbed IgG2a was completely eluted with 100 mM sodium citrate at pH 3. The eluted fractions were then gathered in tubes containing 1 mL Tris-HCl at pH 8 for direct neutralization. The resin was regenerated by applying 2 column volumes of 2 M urea and 2 column volumes of 1 M acetic acid.

## 3. Results and discussion

### 3.1. Flow regime

Visualization experiments to determine the flow regime and the vortex drift velocity were performed with pearl mica particles at 300 cm/h. Stokes' law was used to calculate the mica particle size, the terminal velocity of which is equal to the axial flow rate. A value of 31 µm was obtained. Therefore, pearl mica particles of less than 31 $\mu$m are dragged along with the axial flow while those greater than 31 $\mu$m are fluidized (for flow regime experiments) or go down to their fluidization height (for drift velocity experiments).

Visualization experiments with the silver pearl mica in aqueous suspension (1%) at 300 cm/h were performed at 20, 50 and 75 rpm to observe the laminar Couette and laminar vortex flow regimes (Fig. 2). The pearl mica is made up of anisotropic reflective particles, so with this technique one could easily observe the vortex flow formation throughout the vortex flow reactor. One could also observe the vortex's outflow and inflow boundaries. The boundary between the two vortices moves faster when their outflow boundaries are joined [15], allowing one to see them (Fig. 2b, c and d), but it moves slower when their inflow boundaries are joined [15]; then, it is not possible to visualize them. Hence, a unit is formed by a pair of vortices located between two outflow boundaries. In fact, the unit length could be visually measured, the value being around 0.9 cm (Fig. 2d), twice the size of the vortex or annular gap.

The Taylor numbers were estimated for the rotation rate range using the following equation: $Ta = (\omega \cdot r_i \cdot d)/\nu$, where $\omega$ is the angular velocity, $r_i$ is the inner cylinder radius (m), d is the annular gap (cm), and $\nu$ is the kinematic viscosity ($m^2/s$). The results are shown in Table 2.

The critical Ta number [7] for producing vortices, $Ta_c$, can be estimated using Eq. (1):

$$Ta_c = 41.02 \cdot \left(\frac{d}{r_i}\right)^{-0.5} + 25.75\left(\frac{d}{r_i}\right)^{0.5} + 1.85 \cdot \left(\frac{d}{r_i}\right)^{1.5} \quad (1)$$

For the VFR configuration used in this work, the corresponding critical Taylor number was 69.

To normalize the rotation rate effect as a function of the VFR's geometry and the fluid's physical properties, the $Ta/Ta_c$ ratio was calculated (Table 2).

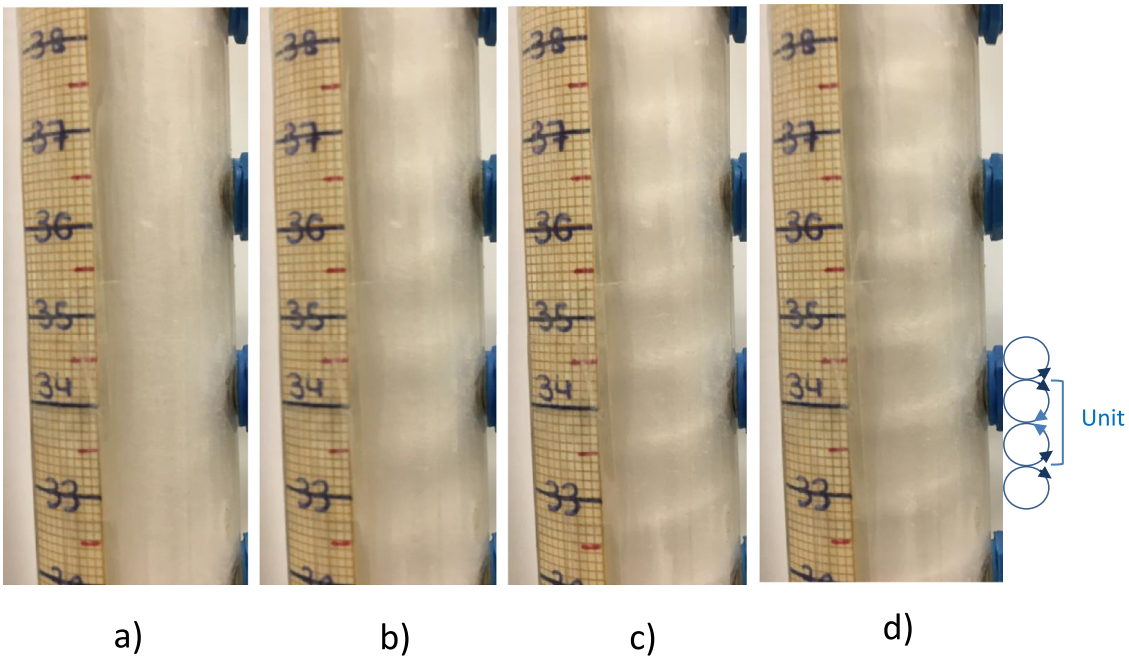


**Fig. 2.** Visualization experiments made with silver pearl mica (1% w/w) in aqueous suspension at 300 cm/h. a) 20 rpm, laminar Couette flow b) 35 rpm, laminar vortex flow c) 50 rpm, laminar vortex flow and d) 75 rpm, laminar vortex flow.

**Table 2**
RTD study results, mass transfer values and regime behavior in the EB-VFR for various rotation rates at 300 cm/h and an expanded bed height (or water height) of 47 cm.

| rpm | Regime* | Adsorbent | Ta | Ta/Ta$_c$ | D$_{ax}$ (m$^2$/s) | Pe | T (min) | K$_{mf}$** (m/s) |
|---|---|---|---|---|---|---|---|---|
| 20 | C | r ProteinA | 49 | 0.7 | $1.2{\cdot}10^{-5}$ $\pm 1{\cdot}10^{-6}$ | 44±4 | 12.3 | $3.5{\cdot}10^{-7}$ |
| 35 | T | r ProteinA | 83 | 1.2 | $1.2{\cdot}10^{-5}$ $\pm 1{\cdot}10^{-6}$ | 44±1 | 12.4 | $4.2{\cdot}10^{-7}$ |
| 50 | T | r ProteinA | 117 | 1.7 | $1.4{\cdot}10^{-5}$ $\pm 3{\cdot}10^{-6}$ | 42±6 | 12.3 | $4.8{\cdot}10^{-7}$ |
| 75 | T | r ProteinA | 177 | 2.5 | $1.6{\cdot}10^{-5}$ $\pm 3{\cdot}10^{-6}$ | 30±6 | 12.7 | $5.5{\cdot}10^{-7}$ |
| 40 | T | no resin | 94 | 1.4 | $7.1{\cdot}10^{-6}\pm 3{\cdot}10^{-7}$ | 55±4 | 14.4 | $4.0{\cdot}10^{-7}$ |

*Regime behavior: Couette flow (C), Taylor flow (T).
** Moore's correlation.

At 20 rpm (Ta/Tac = 0.7), the laminar Couette flow is superimposed on the axial flow in the annulus; this is also called the Couette-Poiseuille flow (Fig. 2a).

Above 35 rpm, the experiments were conducted in the laminar vortices flow regime, where Ta<15·Ta$_c$ [34] (Fig. 2b, 2c and 2d). In this regime, the laminar vortices move upstream with the axial flow. The Reynolds number was calculated as detailed in the bibliography [13], having a value of 5.5 at 300 cm/h. According to Giordano et al. [15], the presence of an axial flow could induce a delay in the vortices onset. However, in our work, this effect was negligible for a Reynolds number of 5.5. Likewise, Lueptow et al. [35] found that laminar vortices appear unaffected up to a Reynolds number of 9.

The vortex drift velocity is defined as the unit core speed divided by the bulk axial flow rate. In this work, the unit's relative speed was measured for all the rotation rates (35-75 rpm) using red pearl mica suspension (1%) injected into the unit (a pair of vortices). The smaller red pearl particles (less than 31 $\mu$m) move inside the unit, making it easier to measure the speed of the pair of vortices, whereas the particles greater than 31 $\mu$m drop to the bottom. The drift velocity was calculated as 1.2±0.1 (a radius ratio of 0.53), so the continuous units displace slightly faster than the axial flow velocity in the laminar vortex flow regime; this is in accordance with the visual flow regime experiments. Furthermore, in the bibliography on the laminar vortex flow regime, the drift velocity tends to be around 1.2 for a radius ratio of 0.95 [36], or between 1 and 1.4 for a radius ratio of 0.85 [35]. In addition, the drift velocity increased when the flow regime changed to a helical vortex flow by increasing the rotation rate (1.5-1.8) [35]. The transition from a laminar to a helical vortices regime for a radius ratio of 0.5 (similar to our VFR) would occur with an axial Reynolds number above 24 [35]. This confirms the laminar vortex flow regime in our VFR, operating at a Reynolds number of 5.5 and Ta/Tac ratios below 2.5.

### 3.2. Expanded bed characteristics in the EB-VFR

In accordance with the bibliography [13], the experiments were conducted at a constant flow rate of 300 cm/h between the minimum and terminal fluidization velocities using Streamline rProtein A.

The terminal fluidization velocity, u$_t$, for the smallest beads can be estimated using Stokes' law as having a value of 364 cm/h. The minimum fluidizing velocity, u$_{mf}$, is calculated using the Levenspiel Eq. [37], giving a value of 9.7 cm/h.

At 300 cm/h, the expanded bed's height was always 47 cm. At low rotation rates of between 35 and 75 rpm (Talt;3·Ta$_c$), the particle suspension was primarily generated by axial flow (Re = 5.5) rather than by the rotation rate (Ta between 83 and 177). Hence, the expanded bed height only depends on the axial velocity. The same VFR behavior was found in the bibliography in reference to hydrodynamic studies focused on purifying BSA [18] and B-phycoerythrin from a concentrated extract of disrupted cells [13].

From the adsorbent mass balance between the settled and expanded bed height, and assuming that the settled bed porosity is 0.4, an expanded bed porosity of 0.75 was determined.

### 3.3. RTD, fluid dynamics and mass transfer in the EB-FVR

The RTD studies were calculated experimentally for a range of low operating rotation rates (20-75 rpm) at a constant expanded bed height (47 cm) and axial velocity (300 cm/h) to explore the hydrodynamic behavior of the EB-FVR using Streamline rProtein A (50 mL).

Table 2 also shows the Péclet number, which is a measure of the overall axial dispersion and thus indicative of the flow through the system as either plug flow or well-mixed, giving a clear idea of the EB-VFR's hydrodynamic behavior in terms of antibody adsorption. The vortices' width was approximately 0.45 cm for this EB-VFR design, corresponding to the annular space. Based on the bed height and vortex height, one can estimate that there were 104 vortices. Knowing that a pair of vortices behaves as a mixed tank, and that their size is approximately twice that of the annular gap [34], there were 52 continuous mixed tanks inside the annular zone, so plug flow can be assumed. When the value of Pe>20, there is plug flow through the expanded bed, and thus it behaves like a packed bed [38].

The EB-VFR behaved as a plug flow reactor at low rotation rates (35 - 75 rpm) and the Pe number was similar, at around 44, for Ta/Tac values close to 1 (between 0.7 and 1.7). The Péclet number began to decrease as the rotation rate increased, with Ta/Tac values greater than 1.7. This accords with the findings of Ma and Cooney [12] for Streamline DEAE, where they reported that an increased rotation rate increases the turbulence within and between vortices so that it is detrimental to the plug flow regime. In Table 2, one can also see that the axial dispersion coefficient ($D_{ax}$, $m^2/s$) at 300 cm/h was not very sensitive to changes in the low rotation rate range. Within the Taylor vortex flow regime (0<Ta/Tac<15), the axial dispersion coefficient was slightly higher than $1 \times 10^{-5}$ ($m^2/s$), suggesting that the expanded bed vortex flow reactor should be unstable, as predicted for an expanded bed column [39]. However, the vortices stabilize the expanded bed and can be used successfully, thus providing the best operating conditions for Ta/Tac values between 1.2 and 1.7.

Observations from another research work [40] suggest that axial dispersion falls to a minimum close to the onset of Taylor vortices and rises along with increasing Taylor numbers (Ta). In that research paper, with rotation rates between 20 rpm and 35 rpm, the dynamic fluid was almost the same, with a Pe number of 44. However, the flow regimes were totally different because at 20 rpm, the laminar Couette flow was present, while at 35 rpm, the laminar vortices regime flow was observed (Fig. 2). Due to the presence of the vortices, the external mass transfer was higher in the laminar vortex flow regime than in the laminar Couette flow regime; accordingly, the adsorption process was carried out above $Ta_c$. The external mass transfer ($k_{mf}$, m/s) for each rotation rate was also determined (Table 2) using Moore's correlation [41], which has been explained in detail by Ibáñez and Cooney [18]. In this case, the molecular weight of the IgG2a (150000 Da) was used to calculate the molecular diffusion coefficient ($D_m$), the value being $4.1 \cdot 10^{-11}$ $m^2/s$.

As shown in Table 2, the external mass transfer increased with increased rotation. This was also due to the unit's increasing outflow boundary speed - the faster it was, the thinner the outflow boundaries [15] (Fig. 2). Table 2 also indicates that, when the axial rate is kept constant, the RTD (T, min) does not depend on the rotation rate, irrespective of the flow regime.

On the other hand, when there is no resin, the tracer must travel further, and the residence time increases (Table 2). Furthermore, the absence of resin increases the Pèclet number up to 55 (at 40 rpm). The adsorbent particles in the expanded bed disFig. the outflow boundaries between the vortices-pair units, increasing the axial mixing (a Pèclet number between 42 and 44). During the RTD analysis or the adsorption step in the expanded bed (Fig. 1a or Fig. 3, step 3), it is not possible to visualize the vortices pairs because the rProtein A beads are not anisotropic reflective particles. However, Giordano et al. [15] concluded that no matter the kind of particles, the flow pattern remained the same.

Comparing the Pe number reported in this paper to those reported in the bibliography [13] with the same $Ta/Ta_c$ ratio of 2.5, one can see that for the H/d aspect ratio reported in this work (104), the calculated Pe was 30, whereas for the reference, the Pe was 44 (with an aspect ratio of 127). However, there were two differences between these two hydrodynamic experiments - the VFR resin volume (50 mL and 135 mL) and the type of adsorbents (Streamline rProtein A and Streamline DEAE), which produced different expanded bed heights, while the settled bed height (20 cm), annular gap (0.45 cm) and axial velocity (300 cm/h) were the same. Therefore, the difference in the Pe number between the two experiments strongly suggests that the higher the aspect ratio, the greater the number of vortices, thus improving the plug flow behavior and the possibility of scaling up the VFR by a factor of 2.7.

According to Curran and Black [42], the vortex flow reactor used as a bioreactor could be successfully scaled up. They selected the annular gap, whereas the Taylor number and L/d were kept constant. Their research focused on keeping the number of vortices pairs or mixed tanks constant in the vortex flow reactor. In contrast, the scaling up of the chromatography column is based on increasing the column diameter while the column's length and superficial velocity are kept the same, as are the residence time and the theoretical plate number in the column. Thus, the scaling up of the vortex flow reactor focused on chromatography should consider all these parameters. A possible solution would be to choose the desired annular gap for the scaling up (increasing the inner and outer cylinders) while keeping the superficial velocity, EB-VFR length, aspect ratio, and $Ta/Ta_c$ constant. In this way, the number of continuous mixed tanks or theoretical plates in the EB-VFR is kept constant. Further research had to be carried out with regard to increasing the scaling-up factor.

The external mass transfer was theoretically compared using Fanś correlation for fluidized bed columns [43] and Moore's Eq. for the VFR, at 300 cm/h using Streamline rProtein A as the adsorbent, IgG2a as the protein and 0.79 as the bed porosity for the culture broth. The external mass transfer calculated in the expanded bed column, $3.7 \cdot 10^{-6}$ (m/s), was higher than the $4.2 \cdot 10^{-7}$ (m/s) for the EB-VFR and the calculated values in Table 2. However, Ibáñez and Cooney [18] obtained better results in the VFR using another protein (BSA) and adsorbent (Streamline DEAE), when the ratio between the annular gap and the inner cylinder, $d/r_{i,}$ was below 0.2. Moore's correlation has two extra variables: the $d/r_i$ ratio and the rotation rate, which can vary the external mass transfer coefficient and improve it.

The dimensionless Biot number $B_i = k_{mf} \cdot d_p / D_p$ was estimated to know if the adsorption process is limited by external mass transfer or by the pore diffusion stage, where $d_p$ is the average particle size (123 $\mu$m), and $D_p$ ($m^2/s$) is the pore diffusion coefficient estimated by the following correlation [44] $D_p = (\varepsilon_p/2 - \varepsilon_p)^2 \cdot D_m$, $_p$ being the porosity of the solid particles (0.5 was chosen in this work). A Biot number of 11.2 was obtained using the lowest external mass transfer coefficient ($4.2 \cdot 10^{-7}$, m/s), which indicates that pore diffusion limits the adsorption process. This result agrees with the literature data [13,18]. Although the external mass transfer is lower in the EB-VFR, the adsorption process is efficient. Even if external mass transfer limits the adsorption process, the VFR should

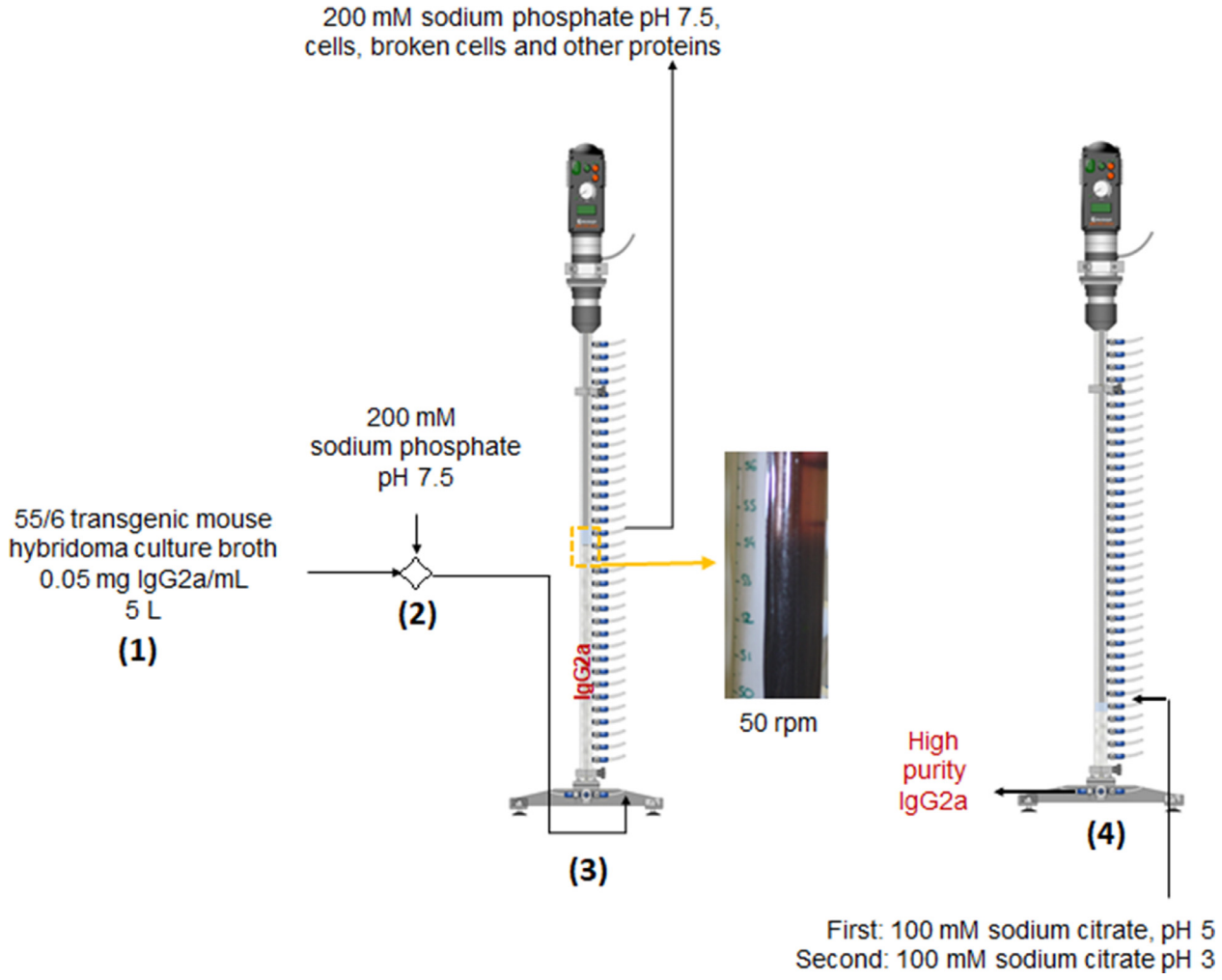


**Fig. 3.** Flowchart for the purification of IgG2a: (1) hybridoma culture from bioreactor; (2) mixing; (3) IgG2a adsorption in EB-VFR; and (4) pure IgG2a elution in settled bed-VFR.

be built with a $d/r_i$ ratio of around 0.2, choosing the highest rotation rate that admits plug flow behavior, thus ensuring higher mass transfer than an expanded bed column.

The Pèclet number was compared between the expanded bed VFR (Table 2) and the column. A Pèclet value of 15 was reported for an expanded bed column using Streamline rProtein A at close to 300 cm/h [45]. In this case, higher values were obtained (42-44) at 300 cm/h due to the extra variable (the rotation rate). The VFR has the advantage of the vortices generating a fairly stable expanded bed. However, it is a challenge to avoid channeling and dead spaces in the expanded bed columns with perforated plates and mesh [46]. A better system, namely the rotating fluid distributor, was designed by Hubbuch et al. [47] to obtain a stable expanded bed. Nevertheless, it still needs to use robust particle adsorbents to avoid them being broken by the rotating cylindrical distributor blades. In contrast, the vortex flow reactor can work with all kinds of adsorbents designed for expanded beds and at all rotation rates because the vortices generated are softer for the particle beads.

### 3.4. IgG2a purification using a vortex flow reactor

During the adsorption process, 5L of cell culture with an IgG2a concentration of 0.05 mg/mL was introduced under the following operating conditions: axial flow rate (300 cm/h), rotation rate (50 rpm) and rProtein A volume (50 mL); these were chosen based on the criteria described below.

The axial flow rate (300 cm/h) was selected following the suggestion of Thömmes et al. [45]. They employed a minimum flow rate, above 300 cm/h, to develop a stable expanded bed column for isolating monoclonal antibodies with Streamline rProtein A.

The inner cylinder's rotation rate was chosen considering the Newtonian behavior of the cell culture's viscosity. Experiments showed a linear relationship between the shear stress and the shear rate, with n at around 1. The calculated flow index value was 1.02 and the average viscosity value for different viscometer speeds (50-90 rpm) was 1.26 mPa·s. Therefore, the rotation rate does not affect the cell culture viscosity, which remains constant. The mass transfer only increases with an increased rotation rate or increased turbulence within or between the vortices.

One can see from Eq. (4) that the Ta number strongly depends on the kinematic viscosity. Consequently, the cell culture density was also measured (1150 kg/m$^3$). For the same rotation speed, increased viscosity can cause the Ta number to drop below the critical $Ta_c$ value at which the vortices regime disappears. The cell culture viscosity value is always greater than the water viscosity value so an inner cylinder rotation rate above 35 rpm was chosen to establish the vortices (in this case 50 rpm), with a Ta number of 118 and a $Ta/Ta_c$ ratio of 1.5. Likewise, a broth with a higher kinematic viscosity could be used, increasing the rotation rate up to a similar $Ta/Ta_c$ ratio of 1.5. During the adsorption process, the IgG2a

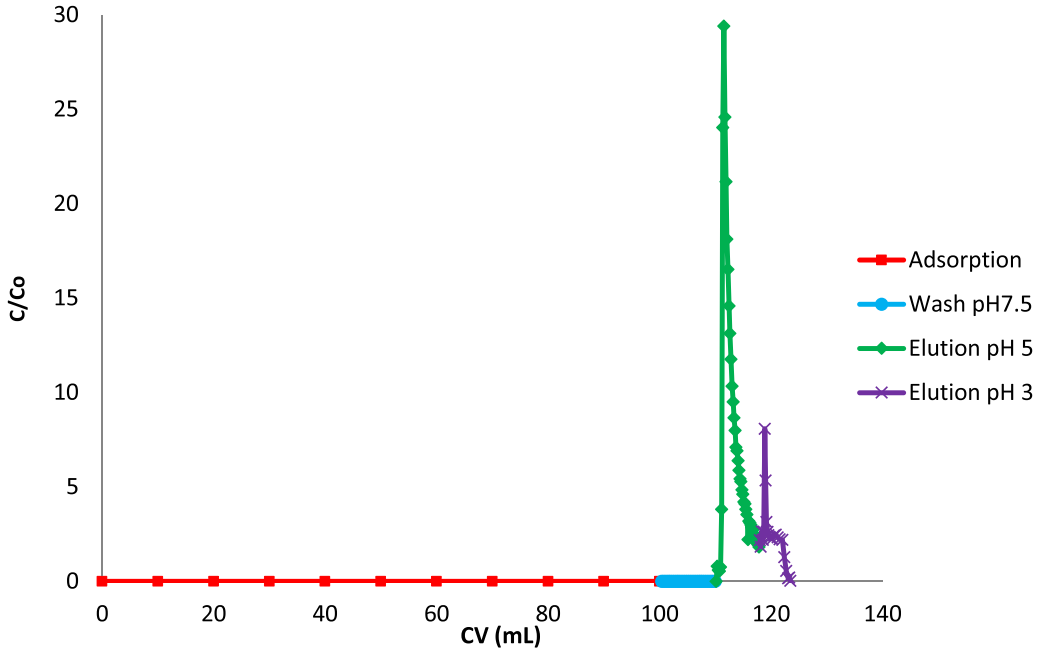


**Fig. 4.** C/Co (Concentration of IgG2a at the outlet divided by the feed concentration) versusthe column volumes (CV) during all the process stages (adsorption and wash at pH 7.5, first elution at pH 5 and second elution at pH 3).

concentrations in the feed and the EB-VFR outlet collecting tubes were determined by Elisa assays.

The C/Co is the ratio between the IgG2a concentration at the VFR outlet (C) and the initial feed concentration (Co) during the various stages: the adsorption and wash in the expanded bed and the elution in the packed bed. This is represented against the number of column volumes in Fig. 4, which refers to the resin volume (50 mL) during the IgG2a purification process.

Under these operating conditions ($Ta/Ta_c$ 1.5 and Re 3.8), one could observe from the visual and hydrodynamic experiments that the EB-VFR worked in the laminar vortex regime and behaved as a plug flow reactor (the Pe number being between 42 and 44) during the adsorption process. All the IgG2a was adsorbed in the resin so the Elisa assay (with a limit of detection below 6.25 ng of IgG2a/mL) could not detect an IgG2a concentration at the outlet. The dynamic capacity, defined as the amount of IgG2a adsorbed in a milliliter of resin, was calculated as 5 mg/mL. The productivity per cycle was defined as the dynamic capacity per volume of resin - a value of 250 mg IgG2a per cycle. The IgG2a adsorption in the EB-VFR took eight hours. It would be possible to decrease the adsorption time by increasing the IgG2a concentration in the feed, which would also increase the dynamic capacity and productivity. The height of the expanded bed was 54 cm; hence, under the established conditions, the number of vortices along the VFR length was 120 (60 continuous pairs of vortices or mixed tanks), which created a plug flow during the adsorption. Although the culture's density and viscosity values were only slightly higher than the physical properties of the equilibrium buffer, the expanded bed height increased by 7 cm during the adsorption stage. This can be attributed to the presence of cells ($5 \times 10^6$ cells/mL) as the expanded bed height depends on the fluid's physical properties and the particle concentration. After the feed was introduced, equilibration buffer was used to clean the resin contained in the EB-VFR until no protein or particles were detected.

A frontal analysis was performed in the expanded bed column to determine the elution pH. The bound antibodies (1.5 mg of IgG2a per 1 mL of resin) were eluted at 150 cm/h with 100 mM of sodium citrate buffer at continuously decreasing pH values, starting at pH 6 and ending at pH 3, looking for the highest pH value to avoid strong neutralization. Table 3 shows the amount eluted at each pH and the percentage of IgG2a recovered with respect to the total amount of IgG2a eluted across all the pH values. The greatest amount of IgG2a was eluted at pH 5, so this value, followed by pH 3, was chosen for the elution process.

**Table 3**
Amount of IgG2a harvested and the yield from the total amount introduced for each elution fraction in the frontal analysis of the expanded bed column.

| pH | ug IgG2a | Yield (%) |
|---|---|---|
| **6** | 166.77 | 10.7 |
| **5** | 1271.60 | 81.9 |
| **4** | 64.72 | 4.2 |
| **3** | 48.99 | 3.2 |
| **All pH** | 1552.08 | 100 |

**Table 4**
Volume, IgG2a amount, and IgG2a yield in each VFR purification step: adsorption and wash in EB-VFR, and the elution (pH 5 and 3) in the settled-bed VFR.

| Purification stages | Volume (mL) | mg IgG2a | IgG2a Yield (%) |
|---|---|---|---|
| Feed | 5000 | 250 | 100 |
| Adsorption | 5000 | 0 | 0 |
| Wash | 250 | 0 | 0 |
| Elution pH5 | 520 | 188 | 75.1 |
| Elution 2 pH3 | 370 | 44.8 | 17.9 |
| ΣElution pH5 + Elution pH3 | 890 | 232.8 | 93.1 |

During the elution step in the VFR's settled bed, 188 mg of IgG2a were obtained at pH 5 (see Table 4). The product eluted from the column was more concentrated, more than 7-fold higher than the starting material (Fig. 4). The yield was calculated at 75.1 percent. The top of the peak eluted at pH5 reached a $C/C_0$ of 30, corresponding to a recovery of 24.6% and 61.42 mg of IgG2a. The highest concentration achieved in the elution fraction was 1.47 mg IgG2a/mL. During the elution, 44.8 mg of IgG2a were recovered at pH 3, which represents 17.9 percent of the initial IgG2a. Between the two peaks, an IgG2a yield of 93.1 % was recovered.

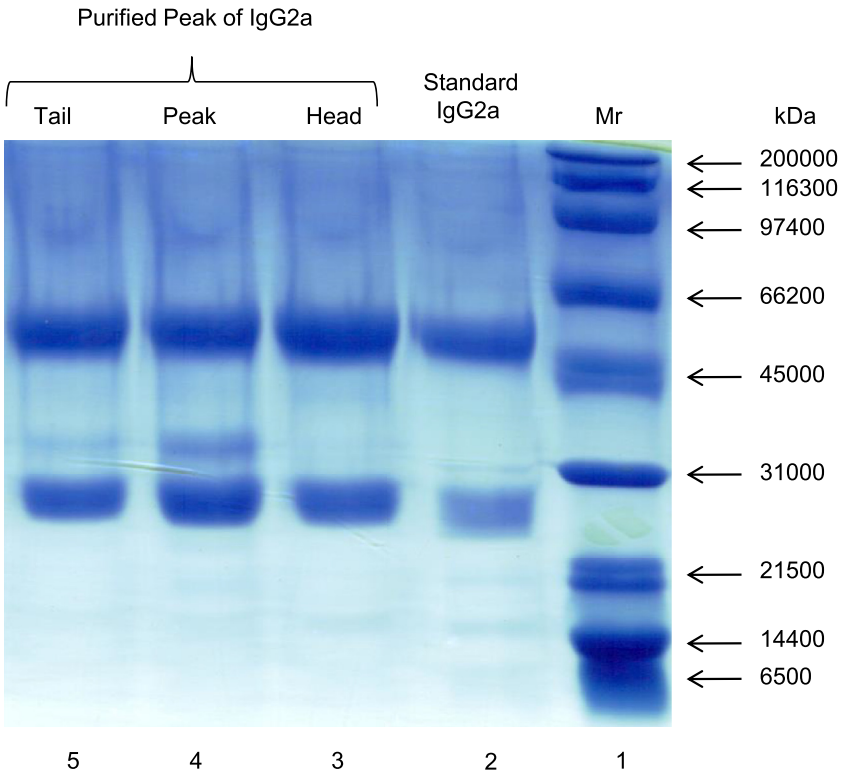


**Fig. 5.** SDS-PAGE gel of antibody fractions to evaluate the purity of the IgG2a in the VFR elution step. Lane 1: molecular weight markers, 3-200 kDa; Lane 2: IgG2a antibody standard; Lanes 3, 4 and 5: antibody purified at pH 5.

### 3.5. Purity of the eluted fraction

The results from the Mouse Immunoglobulin Isotyping ELISA analysis of the culture only detected the presence of IgG2a. The SDS-PAGE analysis (Fig. 5) was carried out to confirm the purity of the fractions obtained during the elution step. The fractions obtained in the elution at pH5 (lanes 3, 4 and 5) were analyzed and compared with a pure IgG2a antibody standard and front molecular weight markers. The SDS-PAGE analysis results showed high IgG2a purity for the fractions obtained in the elution at pH 5, higher for the head and tail than for the peak. Both the Isotyping and the SDS-PAGE analyses, along with the IgG selectivity of the rProtein A resin, confirmed high IgG2a antibody purity eluted at pH 5, which can be extrapolated to the eluted IgG2a antibody fraction at pH 3. In addition, this allowed us to measure the antibodies in the elution stage using the standard IgG2a antibody calibration.

Finally, Table 5 compares the yield and purity achieved in the antibody purification process using the VFR with other technologies. Using Protein A in the VFR seems to be a better option for obtaining highly pure antibodies in a single stage, involving adsorption and elution steps, compared to the other techniques investigated. González et al. [48] used an expanded bed column with Protein A without a prior clarification stage; they achieved a similar yield as in our work and a higher purity. However, they confirmed that the presence of DNA, released by the lysed hybridoma cells, can block the mesh at the column inlet. In the VFR, this drawback is avoided because the inlet is a hole (2 mm in diameter) that cannot be blocked by the presence of DNA or any other impurity. Also, when the process rate is analyzed, namely the relationship between the treated feed volume and the total process time (including the adsorption, washing and elution times), the VFR device used in this work achieved a process rate (7.4 ml/min) that was three-times higher than that achieved in the González research, which used expanded bed adsorption technology (2.4 ml/min). Moreover, the VFR process time could be longer when working with more viscous broth - here, the expanded bed and traditional column cannot compete due to blocking issues and the high pressure.

### 3.6. Viability of the expanded bed vortex flow reactor

The productivity, defined as the number of antibodies per liter of resin and per hour (P, g /(h·L), is calculated using Eq. $P = Q_{10\%}/t_p$, where $Q_{10\%}$ is the dynamic capacity for C/Co = 0.1 and $t_p$ (h) is the processing time. The productivity of our equipment (EB-VFR) was compared to a conventional process (a packed-bed column). In the traditional process, the processing time considers both the clarification time ($t_c$, h) and the affinity chromatography time ($t_a$, h), so $t_p = t_c + t_a$. In contrast, for EB-VFR, only $t_p = t_a$ needs to be considered. The polishing stage is not taken into account because it would be the same for both processes, if needed.

The affinity chromatography time ($t_a$, h) involves the preconditioning, equilibration, adsorption, wash, elution and regeneration stages. This was calculated using the modified Swinnen Eq. [50], $t_a = Q_{10\%}/C_0 \cdot u_a + 22CV/u_a$, where the first term is the adsorption time. The second term represents the time for the other chromatography stages, and 22 CV was assumed for the same axial flow rate ($u_a$, CV/h) in the packed bed column. For the EB-VFR, 20 CV was assumed in the second term, where the axial flow rate is the same for the equilibration stage (300 cm/h) but lower for the elution and regeneration stages in the settled bed (100 cm/h).

Swinnen et al. [50] compared five protein A affinity resins for the purification of monoclonal antibodies. They analyzed the dynamic capacity ($Q_{10\%}$) for the upper and lower linear flow rates of the resin's operating range. The cell culture (Co = 0.68 hIgG/L) was clarified consecutively with a depth filter at 150 L/h·m$^2$ (0.027 m$^2$ for the lab-scale, as indicated by the manufacturer) and an absolute 0.22 $\mu$m filter (18 mL/min·cm$^2$ and a 13 mm diameter,

**Table 5**
Antibody yield and purification factors from the various purification processes.

| Purification system | Steps | Procedure | Antibody | Process yield (%) | Purity (%) | Reference |
|---|---|---|---|---|---|---|
| Vortex flow reactor / Protein A | Single | 1. Vortex flow reactor with Protein A | IgG2a | 93.1 | High Purity | This work |
| Expanded bed column/ Protein A | Single | 1. Expanded bed with Protein A | IgG2a | 85 | High Purity | [45] |
| Expanded bed column/ Protein A | Single | 1. Expanded bed with Protein A | IgG2b | 92 | 98 | [48] |
| Aqueous two-phase system | Multiple | 1. Mixing<br>2. Incubation overnight<br>3. Centrifugation<br>4. Aqueous two-phase system | IgG | 97 | 95 | [28] |
| Phenylboronic chromatography | Multiple | 1. Cell-culture clarification<br>2. Multimodal chromatography | IgG | 97.7 | 82.6 | [31] |
| Integrated purification platform | Multiple | 1. Activated carbon<br>2. Cation exchange chromatography<br>3. Anion exchange chromatography | IgG1 | > 80 | > 98 | [49] |

**Table 6**
Axial flow rate, dynamic capacity, clarification and chromatography processing times and productivity for the different adsorbents from the clarified cell culture in the packed-bed column (0.68 hIgG/L).

| | $u_a$* | | | | | |
|---|---|---|---|---|---|---|
| Adsorbent | cm/h | CV/h | $Q_{10\%}$**(g/L) | $t_c$ (h) | $t_a$ (h) | Productivity (g/L·h) |
| Prosep vA Ultra resin | 500 | 25.0 | 43.5 | 3.4 | 1.2 | 9.4 (6.6) |
| Prosep A High Capacity | 500 | 25.0 | 28.6 | 2.6 | 0.8 | 8.6 (6.2) |
| MabSelect | 300 | 15.1 | 40.1 | 5.4 | 1.1 | 6.2 (4.9) |
| MabSelect Xtra | 200 | 10.3 | 60.1 | 10.7 | 1.6 | 4.9 (4.0) |
| Rmp Protein A Sepharose 4FF | 200 | 10.3 | 37.7 | 7.5 | 1.0 | 4.4 (3.7) |

The values in parentheses are the productivity calculated for an adsorbent volume of 50 mL, keeping the length (20 cm) and axial flow rate constant.
* Average of the upper and lower axial flow rates [50].
** Average of the dynamic capacity at the upper and lower linear flow rates [50].

as indicated by the manufacturer). The data from Swinnen et al. [50] were used to calculate the clarification and the affinity chromatography times, as well as the productivity of these five adsorbents in the packed-bed column, as shown in Table 6. According to the authors, the clarification time increased with an increase in the dynamic capacity or the cell-culture volume. In contrast, the chromatography time decreased, while the productivity increased more by increasing the axial flow rate than by increasing the dynamic capacity. Likewise, the productivity was calculated for 50 mL of adsorbent (the data in parentheses in Table 6) to compare it with EB-VFR productivity. The productivity is reduced because of the increase in the clarification time or the clarified cell-culture volume, whereas the chromatography time remains the same. Hence, the column length and axial flow rate were constant.

The productivity of the EB-VFR (50 mL of Streamline rProtein A) was calculated, giving a low value of 0.40 (g/(L·h). The dynamic capacity (5 mg/mL) was obtained at C/Co = 0 instead of C/Co = 0.1 due to the antibody concentration being low (0.5 mg IgG2a/L) and the adsorption time at 300 cm/h being long (8.1 h); this was the same for the elution time and the regeneration times at 100 cm/h (4.2 h) in the settled bed with no pressure. This productivity was recalculated for an antibody concentration of 0.68 g/L (to compare it with the productivities of the packed-bed adsorbents) and with the optimized values reported for Streamline rProtein A and IgG2a [45], such as a dynamic capacity of 20 mg IgG2a/mL, an axial flow rate of 360 cm/h and an axial elution rate of 150 cm/h. The recalculated productivity increased to 4.0 g/L·h. The affinity chromatography time for EB-VFR dropped from 12.6 h to 5 h but was far from the 1 hour (approx.) for protein A adsorbents in the packed bed (Table 6). Although EB-VFR productivity could compete against the lower axial flow rate adsorbents, it does not do so against the high axial flow rate adsorbent due to the high porosity and pump pressure required to maintain the axial flow rate. To improve EB-VFR productivity, a denser adsorbent is needed to increase the axial flow rate and to provide greater dynamic capacity. These are the so-called second-generation adsorbents [51]. Furthermore, the axial flow rate is kept constant in all the stages because in the expanded bed, the stage performance is around twice that of the settled bed.

Working at industrial scale, 2000 L per batch, the packed column is made up of 14.5 L of adsorbent [52]. At this scale, columns that have a diameter above 30 cm suffer from packing problems that lead to resin compression, edge effect and hysteresis, where dead spaces and different flow rates are created in the column [53]. Moreover, the clarification stage takes eight hours, assuming double filtration [52]; this is in addition to the considerable investment required, the complicated maintenance and the absolute filtration working at pressure. These limitations are even greater when the cell broth is viscous. According to the information reported by Chahar et al. [54], the clarification stage involves costs ranging from 7,000 – 12,000 US$ per batch as well as the use of tangential flow filtration, costing 1,500 US$ per $m^2$. Therefore, using EB-VFR with second-generation adsorbents is an attractive option at the industrial scale, as it avoids these costs and any packing issues. Consequently, future research should focus on scaling-up this process to make it competitive.

## 4. Conclusion

The vortex flow reactor, operating with laminar vortices (with a drift velocity of 1.2) and plug flow hydrodynamic behavior, can successfully purify IgG2a antibodies from unclarified culture. The purification process was carried out employing a single device under very unfavorable conditions, with an unclarified culture broth that had a high impurities content and a low antibody concentration. This technology has overcome the blockage issue, obtaining a high IgG2a yield, seven times more concentrated than in the starting material and with a high purity, as demonstrated by the SDS-PAGE gel assessment. The adsorption unit in an expanded-bed vortex flow reactor is the only operational step required in the process, provided that the adsorbent (rProtein A) exhibits selectivity for the monoclonal antibody of interest. Prior filtration and biomolecule concentration stages are eliminated, leaving a very simple process flow chart employing a single device. Although Protein A adsorbents in packed beds have been improved to provide a high axial flow rate and high dynamic capacity, EB-VFR using second-generation expanded-bed adsorbents offers a good alternative as it avoids the packing issues at large scale as well as the costly investment and maintenance required for the clarification stage. Working with extracellular biomolecules makes the purification process more competitive than purifying intracellular biomolecules, or traditional bioprocesses that need more stages and processing time. The benefits of the vortex flow reactor provide a reliable and effective alternative to the extracellular biomolecule purification process. In addition, it could be considered as a promising prior step to the polishing process. Nonetheless, future research should focus on developing competitive expanded-bed adsorbents (denser and higher dynamic capacity than packed-bed adsorbents) and scaling-up the EB-VFR process.

## Declaration of Competing Interest

Rosa M. Redondo-Miranda, María J. Ibáñez-Gonzalez (corresponding author), Tania Mazzuca-Sobczuk and Emilio Molina-Grima mutually agree to the submission of their manuscript to the Journal of Chromatography A. The authors affirm that: - the Guide for Authors has been consulted in preparing the submitted manuscript, - the manuscript is an original work, - the manuscript has not previously been submitted in other Journal and it is not under consideration for other publications, and - the manuscript is novel in results and findings. Rosa M. Redondo-Miranda, María J. Ibáñez-Gonzalez, Tania Mazzuca-Sobczuk, and Emilio Molina-Grima have read and approved the text and consent to its publication. Almeria University agree to the submission of this paper

## CRediT authorship contribution statement

**Redondo Miranda Rosa M:** Conceptualization, Formal analysis, Investigation, Methodology, Validation, Visualization, Writing – original draft. **Ibáñez González María J:** Conceptualization, Methodology, Supervision, Writing – original draft, Writing – review & editing. **Mazzuca Sobczuk Tania:** Supervision, Writing – review & editing. **Molina Grima Emilio:** Funding acquisition, Supervision.

## Acknowledgments

The research was carried out by members of the BIO-173 Marine Microalgae Biotechnology Research Group of the Andalusian Regional Government (Spain). We would like to thank Ana Cámara-Artigas and her BIO-328 Protein Structures Research Group in the Andalusian Regional Government (Spain) for their support in obtaining the SDS-PAGE analysis.

## Funding

This work was financially supported by the Andalusian Regional Government (Spain), the Spanish Ministry of Science and Innovation and FEDER (EU), P07-CVI-03193, BIO2008-06505 and UAL18-BIO-A016-B1.

## References

[1] S.B. Pawar, B.N. Thorat, CFD simulation of Taylor-Couette flow in scraped surface heat exchanger, Chem. Eng. Res. Des. 90 (2012) 313–322, doi:10.1016/j.cherd.2011.07.012.
[2] W.S. Kim, Application of Taylor vortex to crystallization, J. Chem. Eng. Japan. 47 (2014) 115–123, doi:10.1252/jcej.13we143.
[3] X. Wei, H. Takahashi, S. Sato, M. Nomura, Continuous emulsion polymerization of styrene in a single Couette-Taylor vortex flow reactor, J. Appl. Polym. Sci. 80 (2001) 1931–1942, doi:10.1002/app.1291.
[4] J.S. Kim, D.H. Kim, B. Gu, D.Y. Kim, D.R. Yang, Simulation of Taylor-Couette reactor for particle classification using CFD, J. Cryst. Growth. 373 (2013) 106–110, doi:10.1016/j.jcrysgro.2012.12.006.
[5] T.K. Sengupta, M.F. Kabir, A.K. Ray, A Taylor vortex photocatalytic reactor for water purification, Ind. Eng. Chem. Res. 40 (2001) 5268–5281, doi:10.1021/ie001120i.
[6] M. Subramanian, A. Kannan, Photocatalytic degradation of phenol in a rotating annular reactor, Chem. Eng. Sci. 65 (2010) 2727–2740, doi:10.1016/j.ces.2010.01.004.
[7] S. Lee, R.M. Lueptow, Rotating reverse osmosis: a dynamic model for flux and rejection, J. Memb. Sci. 192 (2001) 129–143, doi:10.1016/S0376-7388(01)00493-8.
[8] G.A. Ameer, S. Raghavan, R. Sasisekharan, W. Harmon, C.L. Cooney, R. Langer, Regional heparinization via simultaneous separation and reaction in a novel Taylor-Couette flow device, Biotechnol. Bioeng. 63 (1999) 618–624, doi:10.1002/(SICI)1097-0290(19990605)63:5⟨618::AID-BIT12⟩3.0.CO;2-3.
[9] H. Masuda, T. Horie, R. Hubacz, N. Ohmura, Process intensification of continuous starch hydrolysis with a Couette-Taylor flow reactor, Chem. Eng. Res. Des. 91 (2013) 2259–2264, doi:10.1016/j.cherd.2013.08.026.
[10] B. Kong, J.V. Shanks, R.D. Vigil, Enhanced algal growth rate in a Taylor vortex reactor, Biotechnol. Bioeng. 110 (2013) 2140–2149, doi:10.1002/bit.24886.
[11] X. Gao, B. Kong, R.D. Vigil, Characteristic time scales of mixing, mass transfer and biomass growth in a Taylor vortex algal photobioreactor, Bioresour. Technol. 198 (2015) 283–291, doi:10.1016/j.biortech.2015.09.013.
[12] J. Ma, C.L. Cooney, Application of vortex flow adsorption technology to intein-mediated recovery of recombinant human $\alpha$1-antitrypsin, Biotechnol. Prog. 20 (2004) 269–276, doi:10.1021/bp0341803.
[13] M.J. Ibáñez-González, T. Mazzuca-Sobczuk, R.M. Redondo-Miranda, E. Molina-Grima, C.L. Cooney, A novel vortex flow reactor for the purification of B-phycoerythrin from Porphyridium cruentum, Chem. Eng. Res. Des. 111 (2016) 24–33, doi:10.1016/j.cherd.2016.03.032.
[14] G.I. Taylor, Stability of a viscous liquid contained between two rotating cylinders, Philos. Trans. R. Soc. A Math. Phys. Eng. Sci. 223 (1923) 289–343, doi:10.1098/rsta.1923.0008.
[15] R.L.C. Giordano, R.C. Giordano, C.L. Cooney, Performance of a continuous Taylor-Couette-Poiseuille vortex flow enzymic reactor with suspended particles, Process Biochem 35 (2000) 1093–1101, doi:10.1016/S0032-9592(00)00143-6.
[16] S. Vedantam, J.B. Joshi, Annular centrifugal contactors - a review, Chem. Eng. Res. Des. 84 (2006) 522–542, doi:10.1205/cherd.05219.
[17] C.M.V. Moore, C.L. Cooney, Axial dispersion in Taylor-Couette flow, AIChE J 41 (1995) 723–727, doi:10.1002/aic.690410329.
[18] M.J. Ibáñez-González, C.L. Cooney, Studies on protein adsorption in a vortex flow reactor, Process Biochem 42 (2007) 1592–1601, doi:10.1016/j.procbio.2007.08.012.
[19] R.M. Lu, Y.C. Hwang, I.J. Liu, C.C. Lee, H.Z. Tsai, H.J. Li, H.C. Wu, Development of therapeutic antibodies for the treatment of diseases, J. Biomed. Sci. 27 (2020) 1–30, doi:10.1186/s12929-019-0592-z.
[20] E. Langer, R.A. Rader, Top trends in biopharmaceutical manufacturing, 2017, Pharm. Technol. 41 (2017) 58–60.
[21] R.N. D'Souza, P.B. Kakarla, V. Yelemane, R. Meyer, P. den Boer, M. Fernández-Lahore, Controlling cell adhesion in antibody purification by expanded bed adsorption chromatography, Sep. Purif. Technol. 183 (2017) 270–278, doi:10.1016/j.seppur.2017.03.002.
[22] J. Zhang, S. Siva, R. Caple, S. Ghose, R. Gronke, Maximizing the functional lifetime of Protein A resins, Biotechnol. Prog. 33 (2017) 708–715, doi:10.1002/btpr.2448.
[23] P.M. Schmidt, M. Abdo, R.E. Butcher, M.Y. Yap, P.D. Scotney, M.L. Ramunno, G. Martin-Roussety, C. Owczarek, M.P. Hardy, C.G. Chen, L.J. Fabri, A robust robotic high-throughput antibody purification platform, J. Chromatogr. A. 1455 (2016) 9–19, doi:10.1016/j.chroma.2016.05.076.

[24] D.E. Ferguson, E.R. Mahan, W. Ma, G. Bitzas, X. Zhong, R. Zollner, A.M. D'Antona, Parallel loading and complete automation of a 3-step mAb purification process for multiple samples using a customized preparative chromatography instrument with networked pumps, J. Chromatogr. A. 1542 (2018) 50–60, doi:10.1016/j.chroma.2018.02.018.
[25] P. Luan, S. Lee, T.A. Arena, M. Paluch, J. Kansopon, S. Viajar, Z. Begum, N. Chiang, G. Nakamura, P.E. Hass, A.W. Wong, G.A. Lazar, A. Gill, Automated high throughput microscale antibody purification workflows for accelerating antibody discovery, MAbs 10 (2018) 624–635, doi:10.1080/19420862.2018.1445450.
[26] W. Becker, A. Scherer, C. Faust, D.K. Bauer, S. Scholtes, E. Rao, J. Hofmann, R. Schauder, T. Langer, A fully automated three-step protein purification procedure for up to five samples using the NGC chromatography system, Protein Expr. Purif. 153 (2019) 1–6, doi:10.1016/j.pep.2018.08.003.
[27] J. Sieberz, B. Stanislawski, K. Wohlgemuth, G. Schembecker, Identification of parameter interactions influencing the precipitation of a monoclonal antibody with anionic polyelectrolytes, Sep. Purif. Technol. 127 (2014) 165–173, doi:10.1016/j.seppur.2014.02.033.
[28] A.M. Azevedo, P.A.J. Rosa, I.F. Ferreira, A.M.M.O. Pisco, J. de Vries, R. Korporaal, T.J. Visser, M.R. Aires-Barros, Affinity-enhanced purification of human antibodies by aqueous two-phase extraction, Sep. Purif. Technol. 65 (2009) 31–39, doi:10.1016/j.seppur.2008.03.006.
[29] M.F.F. Silva, A. Fernandes-Platzgummer, M.R. Aires-Barros, A.M. Azevedo, Integrated purification of monoclonal antibodies directly from cell culture medium with aqueous two-phase systems, Sep. Purif. Technol. 132 (2014) 330–335, doi:10.1016/j.seppur.2014.05.041.
[30] I. Campos-Pinto, E. Espitia-Saloma, S.A.S.L. Rosa, M. Rito-Palomares, O. Aguilar, M. Arévalo-Rodríguez, M.R. Aires-Barros, A.M. Azevedo, Integration of cell harvest with affinity-enhanced purification of monoclonal antibodies using aqueous two-phase systems with a dual tag ligand, Sep. Purif. Technol. 173 (2017) 129–134, doi:10.1016/j.seppur.2016.09.017.
[31] S.A.S.L. Rosa, R. Dos Santos, M.R. Aires-Barros, A.M. Azevedo, Phenylboronic acid chromatography provides a rapid, reproducible and easy scalable multimodal process for the capture of monoclonal antibodies, Sep. Purif. Technol. 160 (2016) 43–50, doi:10.1016/j.seppur.2016.01.002.
[32] O. Levenspiel, The Mean and Variance of a Tracer Curve, Fluid Mech. Its Appl. 96 (2012) 5–10, doi:10.1007/978-1-4419-8074-8_2.
[33] O. Levenspiel, The dispersion model, Fluid Mech. Its Appl. 96 (2012) 47–70, doi:10.1007/978-1-4419-8074-8_6.
[34] K. Kataoka, H. Doi, T. Hongo, M. Futagawa, Ideal plug-flow properties of taylor vortex flow, J. Chem. Eng. Japan. 8 (1975) 472–476, doi:10.1252/jcej.8.472.
[35] R.M. Lueptow, A. Docter, K. Min, Stability of axial flow in an annulus with a rotating inner cylinder, Phys. Fluids A. 4 (1992) 2446–2455, doi:10.1063/1.858485.
[36] H.A. SNYDER, in: Experiments on the stability of spiral flow at low axial Reynolds number, 265, R. Soc. Publ, 1961, pp. 198–214.
[37] O. Levenspiel, Engineering Flow and Heat Exchange, 3rd ed., 2014, pp. 1–398, doi:10.1007/978-1-4899-7454-9.
[38] Y.K. Chang, H.A. Chase, Development of operating conditions for protein purification using expanded bed techniques: the effect of the degree of bed expansion on adsorption performance, Biotechnol. Bioeng. 49 (1996) 512–526 https://doi.org/10.1002/(SICI)1097-0290(19960305)49:5<512::AID-BIT4>3.3.CO;2-X.
[39] P. Li, G. Xiu, A.E. Rodrigues, A 3-zone model for protein adsorption kinetics in expanded beds, Chem. Eng. Sci. 59 (2004) 3837–3847, doi:10.1016/j.ces.2004.06.008.
[40] W.Y. Tam, H.L. Swinney, Mass transport in turbulent Couette-Taylor flow, Phys. Rev. A. 36 (1987) 1374–1381, doi:10.1103/PhysRevA.36.1374.
[41] C.M.V. Moore, Characterization of a Taylor- Couette Vortex Flow Reactor, Massachusetts Institute of Technology, 1994.
[42] S.J. Curran, R.A. Black, Taylor-Vortex bioreactors for enhanced mass transport, Bioreact. Tissue Eng. Princ. Des. Oper. (2005) 47–85, doi:10.1007/1-4020-3741-4_3.
[43] L.-T Fan, Y.-C Yang, C.-Y Wen, Mass transfer in semifluidized beds for solid-liquid system, AIChE J 6 (1960) 482–487, doi:10.1002/aic.690060327.
[44] K. Miyabe, G. Guiochon, Kinetic study of the mass transfer of bovine serum albumin in anion-exchange chromatography, J. Chromatogr. A. 866 (2000) 147–171, doi:10.1016/S0021-9673(99)01127-9.
[45] J. Thömmes, A. Bader, M. Halfar, A. Karau, M.R. Kula, Isolation of monoclonal antibodies from cell containing hybridoma broth using a protein A coated adsorbent in expanded beds, J. Chromatogr. A. 752 (1996) 111–122, doi:10.1016/S0021-9673(96)00504-3.
[46] F.B. Anspach, D. Curbelo, R. Hartmann, G. Garke, W.D. Deckwer, Expanded-bed chromatography in primary protein purification, J. Chromatogr. A. 865 (1999) 129–144, doi:10.1016/S0021-9673(99)01119-X.
[47] J.J. Hubbuch, A. Heebøll-Nielsen, T.J. Hobley, O.R.T. Thomas, A new fluid distribution system for scale-flexible expanded bed adsorption, Biotechnol. Bioeng. 78 (2002) 35–43, doi:10.1002/bit.10170.
[48] Y. González, N. Ibarra, H. Gómez, M. González, L. Dorta, S. Padilla, R. Valdés, Expanded bed adsorption processing of mammalian cell culture fluid: Comparison with packed bed affinity chromatography, J. Chromatogr. B Anal. Technol. Biomed. Life Sci. 784 (2003) 183–187, doi:10.1016/S1570-0232(02)00712-2.
[49] T. Ichihara, T. Ito, Y. Kurisu, K. Galipeau, C. Gillespie, Integrated flow-through purification for therapeutic monoclonal antibodies processing, MAbs 10 (2018) 325–334, doi:10.1080/19420862.2017.1417717.
[50] K. Swinnen, A. Krul, I. Van Goidsenhoven, N. Van Tichelt, A. Roosen, K. Van Houdt, Performance comparison of protein A affinity resins for the purification of monoclonal antibodies, 848 (2007) 97–107. doi:10.1016/j.jchromb.2006.04.050.
[51] R.N.D. Souza, P. Babu, V. Yelemane, R. Meyer, P. Den Boer, M. Fernández-lahore, Controlling cell adhesion in antibody purification by expanded bed adsorption chromatography, Sep. Purif. Technol. 183 (2017) 270–278, doi:10.1016/j.seppur.2017.03.002.
[52] S. Aldington, J. Bonnerjea, Scale-up of monoclonal antibody purification processes, 848 (2007) 64–78. doi:10.1016/j.jchromb.2006.11.032.
[53] U. Gottschalk, Bioseparation in antibody manufacturing: the good, the bad and the ugly, Biotechnol. Prog. 24 (2008) 496–503, doi:10.1021/bp070452g.
[54] D. Chahar, S. Ravindran, S.S. Pisal, Biologicals Monoclonal antibody purification and its progression to commercial scale, Biologicals (2019) 1–13, doi:10.1016/j.biologicals.2019.09.007.